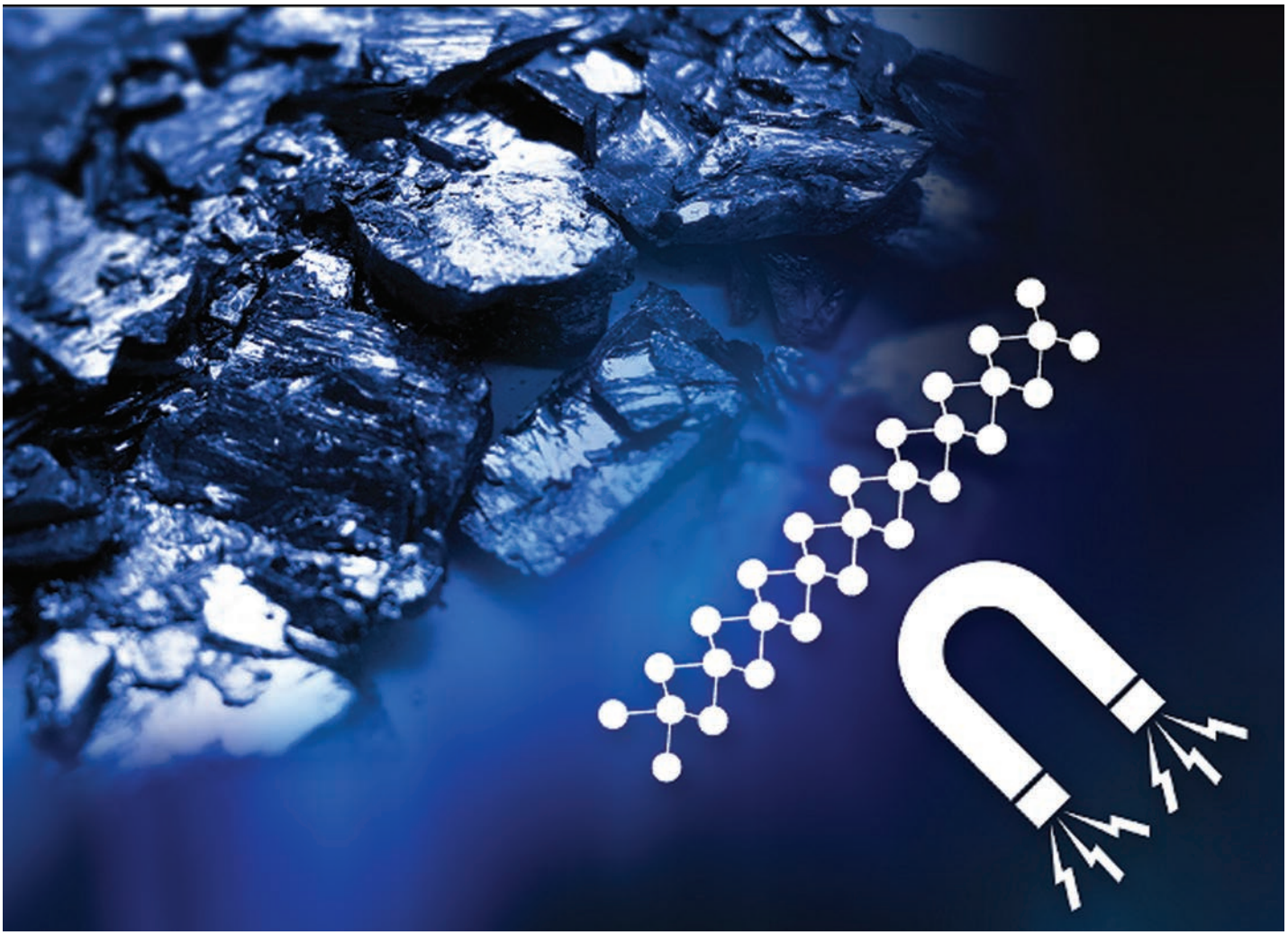

Showcasing research from the Department of Inorganic Chemistry, University of Chemistry and Technology, Prague, Czech Republic.

Title: Origin of exotic ferromagnetic behavior in exfoliated layered transition metal dichalcogenides MoS_2 and WS_2

The room temperature ferromagnetism is closely related to the structural disorder on the sheet edges and the presence of a conductive metallic phase. The origin of room temperature ferromagnetism in transition metal dichalcogenides (TMDCH: MoS_2 and WS_2) was investigated in detail. The ferromagnetism is strongly dependent on the concentration of defects predominantly located on the TMDCH sheets edges as well as on the formation of the metallic 1T phase. Significant differences between the ferromagnetism of TMDCH exfoliated using butyllithium and sodium naphtalenide originate from differences in the exfoliation degree.

As featured in:

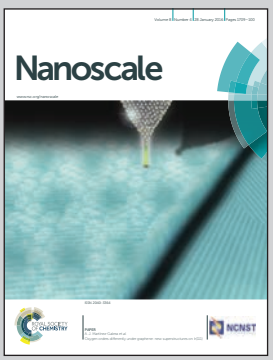

See Zdeněk Sofer *et al.* *Nanoscale*, 2016, **8**, 1960.

ROYAL SOCIETY OF CHEMISTRY

www.rsc.org/nanoscale

Registered charity number: 207890

Nanoscale

PAPER

View Article Online
View Journal | View Issue

Cite this: *Nanoscale*, 2016, **8**, 1960

Origin of exotic ferromagnetic behavior in exfoliated layered transition metal dichalcogenides MoS_2 and WS_2†

Jan Luxa,[a] Ondřej Jankovský,[a] David Sedmidubský,[a] Rostislav Medlín,[b] Miroslav Maryško,[c] Martin Pumera[d] and Zdeněk Sofer*[a]

Received 24th August 2015,
Accepted 21st October 2015

DOI: 10.1039/c5nr05757d

www.rsc.org/nanoscale

Bulk layered transition metal dichalcogenides (TMDs) show diamagnetic properties. When exfoliated, the materials' band gap increases and changes from an indirect band gap to a direct one. During the exfoliation, the TMDs may undergo a phase transition from 2H to 1T polymorph, which is likely electronically driven and accompanied by a metal–insulator transition. A significantly higher efficiency of the exfoliation was observed using sodium naphthalenide compared to butyllithium. Moreover we demonstrate that the exfoliation has a dramatic influence on the magnetic properties of two TMDs, MoS_2 and WS_2. These materials become partly ferromagnetic upon exfoliation, which is a highly unexpected behavior. Exotic ferromagnetism is generally observed on samples with a high degree of exfoliation, which indicates the association of this effect with defects formed on the edges of dichalcogenide sheets. Such an exotic ferromagnetic behavior, if properly understood and brought under material engineering control, shall open the door to new applications of these materials.

Introduction

Layered transition metal dichalcogenides (TMDs) have received revived interest in the past few years being dubbed as the "next graphene" due to their possible applications in energy generation and their highly anisotropic material properties.[1–4] In contrast to graphene, where the layer is single atom thick and truly 2-dimensional, MoS_2 (or WS_2) sheets consist of transition metals sandwiched between two layers of chalcogen atoms. These triple layers are bonded to each other by van der Waals interactions.[5,6] Such a "triple-layer" can exhibit three different crystallographic arrangements, the most common semiconducting 2H (trigonal prism), metallic 1T (octahedral) and semiconducting 3R (trigonal prism).[7,8] The broad selection of metal elements and chalcogens in TMD as well as the large variety of different crystal structures of the materials yield a large number of combinations for tailoring the TMD properties. One of them is the magnetic behaviour. Similarly to graphite, MoS_2 or WS_2 in their bulk forms do not exhibit ferromagnetic or paramagnetic behavior. The magnetic properties of TMDs have been studied both theoretically and experimentally. Theoretically it has been predicted that the introduction of sulphur vacancies onto the S-edges of MoS_2 nanoribbons would lead to a non-zero net magnetic moment.[9] Furthermore zigzag and armchair terminated edges of MoS_2 nanoribbons were studied by density functional theory (DFT) calculations. It was predicted that the zigzag terminated nanoribbons are metallic and show ferromagnetic properties while armchair terminated nanoribbons are semiconducting and nonmagnetic.[10] A magnetic ordering has also been theoretically described for WS_2 nanosheets. The results of DFT calculations have shown that the adsorption of non-metallic elements such as H, B, O or F onto the edges of TMDs induces magnetic properties.[11] More recently experimental studies have been emerging. While the synthesis of magnetic TMD nanoribbons has not been reported, probably because of the difficulties in their synthesis,[12,13] only a few reports on TMD magnetic nanosheets exist. The first report on magnetic MoS_2 nanosheets was based on thermal evaporation synthesis onto silicon or tantalum foil substrates.[14] However the role of the substrate and the interface between MoS_2 and the substrate remains unclear and may have influenced the magnetic properties of the prepared samples.[15,16] Further studies have shown the preparation of MoS_2 by a two-step hydrothermal synthesis, which introduces sulphur vacancies responsible for magnetic behaviour.[17] Magnetic WS_2 nanosheets have also

[a]*Department of Inorganic Chemistry, University of Chemistry and Technology Prague, Technická 5, 166 28 Prague 6, Czech Republic. E-mail: zdenek.sofer@vscht.cz*
[b]*New Technologies - Research Centre (NTC) at University of West Bohemia (UWB), CZ-30614 Pilsen, Czech Republic*
[c]*Institute of Physics of the ASCR, v.v.i., Cukrovarnická 10/112, 162 00 Prague 6, Czech Republic*
[d]*Division of Chemistry & Biological Chemistry, School of Physical and Mathematical Sciences, Nanyang Technological University, Singapore 637371, Singapore*
†Electronic supplementary information (ESI) available. See DOI: 10.1039/c5nr05757d

been prepared by exfoliation in DMF.[18] However, the frequently used organometallic intercalation followed by exfoliation has not been employed for the synthesis of the above mentioned TMD nanomaterials. These methods are easily scalable and relatively undemanding. Here we wish to show that exfoliated MoS_2 and WS_2 exhibit exotic ferromagnetic properties, which we consider as an unexpected behavior in view of the fact that bulk TMDs exhibit diamagnetic properties.

Experimental

Materials

Molybdenum disulphide (99.8%) and tungsten disulphide (99.8%) were obtained from Alfa Aesar. *n*-Butyllithium (1.6 M in hexane), benzophenone and sodium were obtained from Sigma-Aldrich, Czech Republic. Tetrahydrofuran (THF), hexane and naphthalene were delivered by Lach-Ner, Czech Republic. Hexane was dried with sodium before use and THF was dried by distillation from a sodium/benzophenone mixture under an argon atmosphere before use.

Synthesis procedure

The exfoliation of MoS_2 and WS_2 with butyllithium was performed at room temperature. 3 g of MoS_2 was stirred with butyllithium solution for 72 hours. Subsequently the intercalated MoS_2 and WS_2, respectively, were filtered out and washed with hexane. All these operations were performed under an argon atmosphere in a glovebox. Intercalated MoS_2 and WS_2 were dispersed in water and repeatedly centrifuged and redispersed in water. Finally the exfoliated material was dried in a vacuum oven for 48 hours at 50 °C before further use.

Sodium naphthalenide used as an intercalation compound was prepared by stirring sodium metal (0.35 g) with naphthalene (1.8 g) for 2 h in 50 ml of THF under an argon atmosphere. After the addition of transition metal dichalcogenide (TMD) powders (3 g), intercalation was carried out by stirring the solutions at room temperature for 24 h under an argon atmosphere. The prepared intercalates were then suction filtered and washed several times with THF. Separated samples were dispersed in water and centrifuged several times. Finally the exfoliated material was dried in a vacuum oven for 48 hours at 50 °C before further use.

Analytical techniques

Morphology studies were performed by using a scanning electron microscope (SEM) equipped with a FEG source of electrons (Tescan Lyra Dual Beam Microscope). The sample composition was determined by means of an energy dispersive spectroscopy (EDS) analyzer (X-MaxN) with a 20 mm^2 SDD detector (Oxford Instruments). Data were evaluated using AZtecEnergy software. Before the measurement, samples were placed onto a conductive carbon tape to avoid charging effects. All the measurements were carried out with 15 kV acceleration voltage.

High-resolution transmission electron microscopy (HRTEM) was carried out on a transmission electron microscope JEOL JEM 2200FS operated at 200 kV (autoemission Schottky gun, point resolution 0.19 nm) with an in-column energy Ω-filter for EELS/EFTEM analyses, a STEM unit, and an Energy Dispersive X-ray (EDX) SDD detector (Oxford Instruments X-Max attached). Images were recorded on a Gatan CCD camera with a resolution of 2048 × 2048 pixels using the Digital Micrograph software package. EDX analyses were performed and treated with the INCA software package.

High resolution X-ray photoelectron spectroscopy (XPS) was performed with an ESCAProbeP (Omicron Nanotechnology Ltd, Germany) spectrometer using a monochromatic aluminium X-ray radiation source (1486.7 eV). A wide scan survey of all elements was performed with consequent high-resolution scans of the Mo, W and S core levels. Relative sensitivity factors were used to determine the chalcogen-to-metal ratio and the quantitative distribution of 2H and 1T phases. The samples were placed onto a carbon conductive tape prior to the measurement.

Characterization by Atomic Force Microscopy (AFM) was performed on the NT-MDT Ntegra Spectra from NT-MDT in tapping mode. The samples were dispersed in isopropyl alcohol (0.5 mg mL^{-1}), sonicated for 10 minutes and then dropped onto a freshly cleaved mica substrate before the measurement.

An InVia Raman microscope (Renishaw, England) was used for Raman spectroscopy measurements. The spectrometer operates in backscattering geometry with a CCD detector. A Nd-YAG laser (532 nm, 50 mW) was used with 50× magnification objective. The instrument was calibrated on a silicon reference which gives a peak position at 520 cm^{-1}. The laser power did not exceed 5% of the maximum 50 mW power in order to avoid damage to the sample.

The magnetic measurements were performed using a SQUID magnetometer MPMS-XL (Quantum Design). The hysteresis loops were recorded between −10 and 10 kOe at T = 300 K. The magnetization measurements at T = 2 K were conducted between 0 and 70 kOe.

The surface areas were measured using adsorption of methylene blue. About 0.05 g of each TMD material (weighed exactly to within ±0.01 mg) was dispersed in 70 mL of deionized water by ultrasonication (400 W, 30 min). A defined amount of 1 mM of methylene blue aqueous solution was added to the suspension and then filled to 100 mL. The concentration of unabsorbed methylene blue was determined by UV-Vis spectroscopy at λ_{max} = 665 nm (Cary 50, Agilent). For the calculation of surface areas, the value of 1.05 nm^2 per methylene blue molecule was used.[19]

Results and discussion

Here we have investigated the effect of the exfoliation process on the magnetic and structural properties of molybdenum and tungsten disulfide. We have used two agents for chemical exfo-

liation of bulk MoS_2 and WS_2: butyllithium (BuLi) and sodium naphthalenide (NAPH). While butyllithium is commonly used for the chemical exfoliation of transition metal dichalcogenides (TMDs),[20,21] only little has been reported on TMD exfoliation using sodium naphthalenide.[22] Further on, we will show that sodium naphthalenide is not only more efficient in TMD exfoliation than butyllithium for both MoS_2 and WS_2 but also induces magnetic ordering. Before the discussion of exotic magnetic properties of exfoliated TMDs we thoroughly examined the exfoliated TMDs by scanning electron microscopy (SEM), atomic force microscopy (AFM), X-ray photoelectron spectroscopy (XPS), Raman spectroscopy, high-resolution transmission electron microscopy (HR-TEM), selective area electron diffraction (SAED) and surface area measurement by methylene blue adsorption. We will show that the magnetic properties measured by using a superconducting quantum interference device (SQUID) strongly depend on the character and concentration of the induced defects. Simultaneously, the phase transition from the 2H to 1T form, which sets in as a result of intercalation (likely due to charge carrier doping), has to be correlated with the peculiar magnetic behavior.

The morphology of the exfoliated and bulk TMDs was examined by SEM as shown in the ESI (Fig. SI1†). One can observe that for BuLi exfoliated WS_2, most of the sheets remained stacked with sharp edges, indicating an incomplete intercalation and the subsequent exfoliation has been incomplete. It is known that intercalation of Li to WS_2 is incomplete at room temperature and becomes more pronounced at higher temperatures.[23] NAPH exfoliation of WS_2, on the other hand, leads to sheets with smaller lateral sizes and slight edge wrinkling, which points to a significantly higher degree of exfoliation than that in the case of WS_2·BuLi. A similar trend can be observed for MoS_2, however, with more substantial edge wrinkling, especially for NAPH exfoliated MoS_2.

XRD measurements were further conducted (Fig. SI2†) to confirm the presence of pure TMDs. We have not detected any diffraction lines originating from molybdenum or tungsten oxides. This indicates a low degree of oxidation of MS_2 to MO_2/MO_3. Even though some increase in MO_3 was observed by XPS measurements (see XPS discussion), it was only on the surface and was only detectable by XPS. It is also obvious from the data that NAPH exfoliated TMDs show less intense and broadened reflections. This is especially apparent for NAPH·MoS_2 which only shows weak and very broad reflections indicating a high degree of exfoliation. As for NAPH·WS_2 we have detected much higher tendency for restacking (even though AFM and Raman spectroscopy indicate a similar level of exfoliation as for MoS_2 and all XRD measurements were performed within a couple of weeks after preparation) which is obvious from its quite sharp XRD pattern. Also the BuLi exfoliated TMDs show much lower degree of exfoliation which is in good agreement with the data discussed later on.

We used AFM to determine the sheet thickness and to further investigate the morphology of the exfoliated MoS_2 and WS_2. Fig. 1 shows the AFM images documenting that the use of BuLi for exfoliation of MoS_2 and WS_2 leads to multilayered

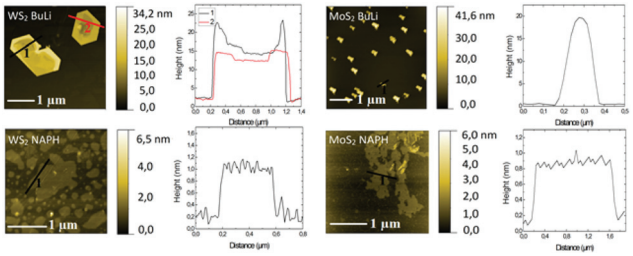

Fig. 1 AFM images of exfoliated transition metal dichalcogenides.

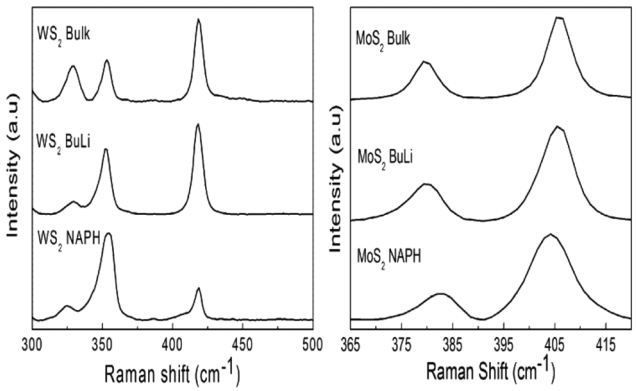

Fig. 2 Raman spectra of exfoliated transition metal dichalcogenides in their bulk state (top), after exfoliation with butyllithium (middle) and after exfoliation with sodium naphthalenide (bottom).

materials with sheet thicknesses of ~20–25 nm. While WS_2 retains its sharp edged structure observed by SEM, MoS_2 consists of sub-micron sized flakes. The application of NAPH led to a high degree of exfoliation of both MoS_2 and WS_2 manifested by a typical sheet thickness (~0.7 nm) corresponding to a single layer. This result is in good agreement with the previously reported values of the monolayer thickness of MoS_2 and WS_2, respectively.[5,24]

To obtain insight into the structural properties of exfoliated TMDs, we performed Raman spectroscopy. It is well known that Raman spectroscopy is a very useful tool for identifying structural properties as well as the number of layers as has been shown several times for various TMDs including MoS_2 and WS_2.[24–26] WS_2 shows two first-order modes denoted as E^1_{2g} and A_{1g} at 356 cm^{-1} and 418 cm^{-1}, respectively and a disorder activated mode denoted as LA at 352 cm^{-1}, which dominates the WS_2 Raman spectrum. These modes can be effectively used to determine the number of layers. Raman spectra show no apparent difference between BuLi exfoliated WS_2 and the spectrum of bulk materials (Fig. 2). This would suggest that the material was delaminated only to a small extent, which is in good agreement with the results previously observed by SEM and AFM. The spectrum of NAPH exfoliated WS_2 shows major differences. We can note the decrease in the $I(A_{1g})/I(E^1_{2g})$ ratio from ~2 in the bulk material to ~0.35 in

NAPH exfoliated WS_2. This has been previously reported as a characteristic feature of a single atom layered WS_2.[24] It should be noticed that the band centered at around 354 cm^{-1} is broadened, which is associated with an activation of LA mode due to disorder introduced during the exfoliation (*e.g.* edge wrinkling observed by SEM and HR-TEM). In addition we have located low intensity peaks in the low frequency region (see Fig. SI3†). These peaks correspond to the 1T phase and are denoted as J_1, J_2 and J_3.[27] Even though these modes confirm the presence of the 1T form since they are not allowed in the 2H phase structure, it is more accurate to use other methods, such as XPS, to calculate the 1T concentrations.[27] It is noticeable that these modes are also visible even in the spectrum of BuLi·WS_2 where AFM and XRD showed a very low, if any, degree of exfoliation. This suggests that even though the intercalation of BuLi into WS_2 and its subsequent exfoliation are highly inefficient, some charge carrier doping takes place, leading to a slight increase in the 1T phase concentration (see XPS for a detailed discussion).

The modes denoted as E^1_{2g} at 383.5 cm^{-1} and A_{1g} at 408.6 cm^{-1} in the spectra of MoS_2 are of analytical value. The peak separation Δ is used in the case of MoS_2 for the determination of the number of layers. We have obtained Δ = 26.1 cm^{-1} for bulk MoS_2 and Δ = 26 cm^{-1} for BuLi exfoliated MoS_2. These values are nearly identical and they signify that the thickness of BuLi exfoliated MoS_2 is more than four layers.[28] By contrast, we have shown by AFM measurements that the average sheet thickness is lower than that of the bulk material. More importantly, NAPH exfoliated MoS_2 shows the peak separation of Δ = 21.4 cm^{-1}. This value is close to that of monolayer MoS_2 documenting that the high efficiency of NAPH was highly efficient in MoS_2 exfoliation.[28,29]

In addition to E^1_{2g} and A_{1g} modes, several additional features can be seen in the low wavenumber region of MoS_2 and WS_2 spectra (see Fig. SI3†). Firstly, modes denoted as J_1, J_2 and J_3 (pink regions) are clearly visible in the spectra of MoS_2·BuLi and MoS_2·NAPH. These modes are not allowed in 2H modification but become allowed in 1T MoS_2 polymorph.[30,31] This indicates a successful 2H to 1T phase transition in BuLi·MoS_2 and NAPH·MoS_2 samples. In the spectrum of bulk MoS_2 none of these modes (J_1, J_2, J_3) can be detected. Even though the presence of J_1, J_2 and J_3 phonon modes prove the presence of the 1T phase, other methods such as XPS are more suitable for determining the relative 1T phase concentrations.[30] The peak at ~280 cm^{-1} is related to the presence of MoO_3.[32] The presence of MoO_3 on the surface has been proven by XPS measurements (see XPS discussion). The increase in the intensity of the peak located at ~280 cm^{-1}, compared to the bulk material, for MoS_2·BuLi and MoS_2·NAPH is likely caused by slightly higher amounts of MoO_3 on the surface of these samples, also observed by XPS.

So far we have shown by means of SEM, AFM and Raman measurements that sodium naphthalenide is more efficient in exfoliation of bulk MoS_2 and WS_2 than the usually used butyllithium. In order to obtain better information on the chemical changes taking place within the prepared materials, we conducted XPS measurements. Detailed high-resolution spectra of core-level Mo 3d and W 4f after Shirley background subtraction are displayed in Fig. 3.

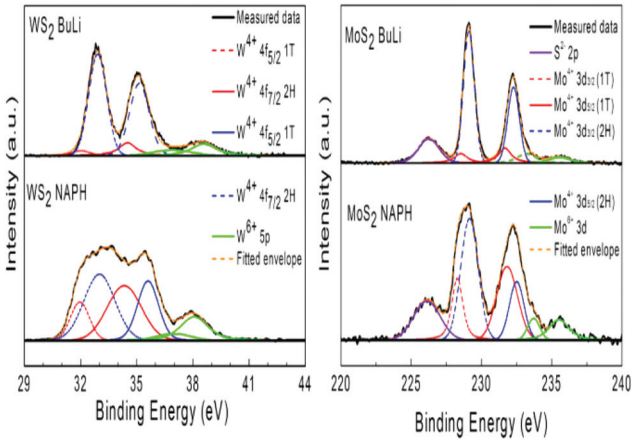

Fig. 3 High-resolution XPS spectra of W 4f in WS_2 and Mo 3d in MoS_2 exfoliated with butyllithium and sodium naphthalenide.

Table 1 Contents of 1T, 2H phase and M^{6+} as obtained from the high-resolution core-level spectra of Mo 3d and W 4f

Sample	1T (at%)	2H (at%)	M^{6+} (at%)
MoS_2·BuLi	15.3	73.3	11.4
MoS_2·NAPH	38.9	48.2	12.9
WS_2·BuLi	10.2	77.8	12.0
WS_2·NAPH	37.1	48.1	14.7

It is well known that bulk materials consist mainly of the semiconducting 2H phase. During the exfoliation varying amounts of metallic 1T phase emerge as a consequence of electron doping introduced during intercalation.[33] The relative changes of the transition from the 2H to 1T phase are summarized in Table 1. For WS_2, the spectra consist of W^{4+} $4f_{5/2}$ and W^{4+} $4f_{7/2}$ peaks at approximately 32 eV and 35.1 eV, respectively, corresponding to the 2H phase. A contribution of the 1T phase can be also found in the spectra at around 31.1 eV and 34.2 eV as well as the pair corresponding to W^{6+} at ~36.8 eV and ~38.5 eV. The deconvolution of those components is essential when trying to identify the chemical changes occurring during the exfoliation.

For BuLi exfoliated WS_2 it is clearly visible that there is only a small contribution from the metallic 1T phase of about 10 at%. This reflects the low degree of exfoliation (and the low degree of electron doping) also supported by electron microscopy and Raman measurements. Then for NAPH exfoliated WS_2 a much more pronounced increase in the 1T phase to ~37% was observed. The presence of W^{6+} is also notable from the spectra for both samples.

Let us note that even in bulk materials there is a certain amount of tungsten atoms (as well as Mo in MoS_2) in the

oxidation state of M^{6+} (see Table SI1†). The slight increase of W^{6+} concentration in NAPH·WS_2 is likely caused by a higher surface area available in the more exfoliated material. Now for MoS_2 the detailed high-resolution core-level spectra can be evaluated in a similar manner as for WS_2. In this case these are the Mo^{4+} $3d_{3/2}$ at ~229.1 eV and Mo^{4+} $3d_{5/2}$ at ~232.5 eV peaks that correspond to the 2H phase. The peaks corresponding to the 1T phase appear at about 0.9 eV lower binding energies (~228.2 eV and ~231.4 eV). Finally Mo^{6+} species are located at approximately 232.7 eV and 235.5 eV. For BuLi exfoliated MoS_2 the 1T phase content is ~15 at% while for NAPH exfoliated MoS_2 it is as high as ~39 at%. The higher amount of Mo^{6+} in NAPH·MoS_2 can be explained in the same way as for WS_2. It is also possible to track chemical changes in molybdenum and tungsten disulphides by deconvolution of the S 2p core-level, but it is rather difficult to determine the changes with satisfying accuracy because of the low proximity and overlap of individual components. The S 2p high-resolution core-level spectra are shown in Fig. SI4.† In addition the survey spectra are shown in the ESI (Fig. SI5†) together with the individual element concentrations (Table SI2†).

The HR-TEM measurement was performed in order to further investigate the structure of exfoliated MoS_2 and WS_2 at the atomic level. The SAED in combination with EDS was applied to confirm the structure and elemental composition of exfoliated TMDs. Both materials, exfoliated with butyllithium and sodium naphthalenide, are composed of both single and few layer sheets. All exfoliated TMDs with the exception of the WS_2·BuLi sample exhibit wrinkling close to the rim of the sheets (Fig. SI6†). The EDS analysis yielded the S/Mo ratio close to the theoretical value of 2 (2.09 for MoS_2·BuLi and 1.93 for MoS_2·NAFT). The EDS analysis of WS_2 exfoliated with butyllithium and sodium naphthalenide gave the S/W ratio of 0.41 and 1.23, respectively. Such a large difference in the S/W ratio can be explained by the large difference in tungsten and sulfur molar mass. The selective area electron diffraction (SAED) was performed on selected sheets of TMDs which were further investigated by HR-TEM microscopy. The diffraction shows the presence of both single and few layer TMDs with the hexagonal symmetry of the structure. The results of SAED are shown in the ESI (Fig. SI7†). The HR-TEM can be used to distinguish between 2H and 1T phases. In order to identify different phases, detailed images were obtained. In comparison with BuLi exfoliated TMDs we can observe a high degree of disorder on the rims of TMD sheets exfoliated with sodium naphthalenide. This can be seen in detail in Fig. 4 for exfoliated MoS_2 and WS_2. The disorder in the MoS_2 and WS_2 structures was theoretically predicted to be responsible for room temperature ferromagnetism[34] and also experimentally reported for MoS_2 layers with a high concentration of edges.[35] Since the samples exfoliated with sodium naphthalenide exhibit a significantly larger degree of exfoliation with a higher concentration of edges and a high degree of disorder, the relationship with the observed room temperature ferromagnetism appears to be quite straightforward.

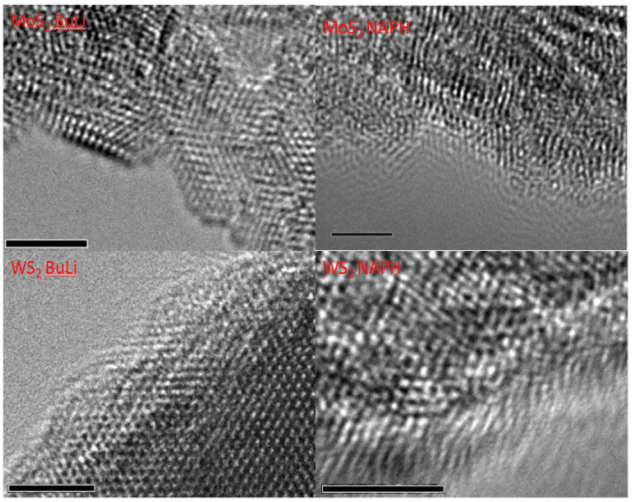

Fig. 4 The defects on the edges of MoS_2 and WS_2 sheets exfoliated with butyllithium and sodium naphthalenide observed by HR-TEM. The scale bar corresponds to 2 nm.

In order to recognize the presence of the 2H and 1T phases from HR-TEM images, we used the method reported in the literature.[30] The MoS_2·NAPH showed the dominant presence of 1T modifications while for the sample MoS_2·BuLi, we can see both the 1T and 2H structures. This is in qualitative agreement with XPS results, where the higher concentration of the 1T phase was observed for samples exfoliated with sodium naphthalenide. The HR-TEM images of exfoliated MoS_2 and WS_2 are shown in Fig. 5.

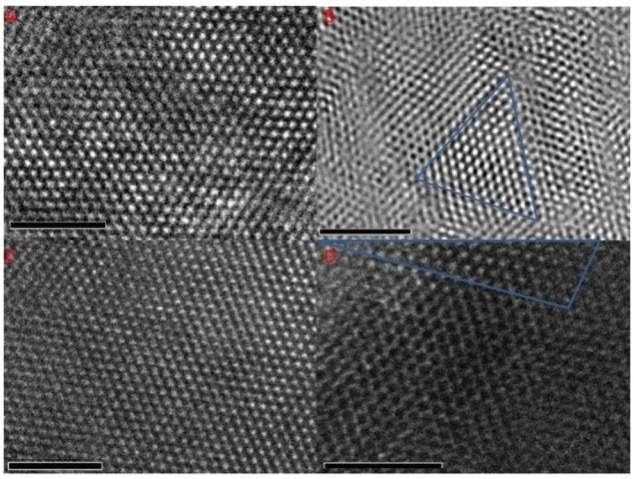

Fig. 5 The HR-TEM images of MoS_2 exfoliated with sodium naphthalenide (A) and butyllithium (B). The dominant occurrence of the 1T form is clearly seen in the MoS_2·NAPH sample (panel A) while for the sample MoS_2·BuLi (panel B) both phases, 2H and 1T (1T phase marked by blue triangle), coexist in comparable amounts. WS_2 exfoliated with sodium naphthalenide corresponds to panel C and with butyllithium to panel D where both 2H and 1T forms can be identified (1T phase marked by a blue triangle). The scale bar corresponds to 2 nm.

Table 2 Summary of magnetization measurements on exfoliated as well as bulk MoS_2 and WS_2

Sample	χ_D (emu (g Oe)$^{-1}$)	m_S (emu g^{-1})	m_{PM0} (emu g^{-1})	χ_1 (emu (g Oe)$^{-1}$)
MoS_2·NAPH	-6.818×10^{-8}	0.0019	0.156	5.311×10^{-7}
WS_2·NAPH	-2.161×10^{-7}	0.0007	0.0164	6.1×10^{-9}
WS_2·BuLi	-3.188×10^{-7}	$<2.0 \times 10^{-5}$	0.045 ($S = 2$)	2.1×10^{-8}
MoS_2·BuLi	-3.551×10^{-7}	$<2.0 \times 10^{-5}$	0.1 ($S = 1$)	4.23×10^{-7}
MoS_2	-3.98×10^{-7}	8.1×10^{-5}	0.0473 ($S = 2$)	2.78×10^{-7}
WS_2	-3.461×10^{-7}	$<2.0 \times 10^{-5}$	0.0266 ($S = 2$)	2.49×10^{-8}

In order to better quantify the degree of MoS_2 and WS_2 exfoliation we performed the surface area measurement using methylene blue adsorption. This method was reported to be useful for surface area measurement of TMDs and other layered compounds such as clay silicates.[36,37] The obtained surface area of MoS_2 and WS_2 exfoliated with butyllithium was 62.1 m^2 g^{-1} and 36.1 m^2 g^{-1}, respectively. A significantly larger area was obtained for MoS_2 and WS_2 exfoliated using sodium naphthalenide, 88.3 m^2 g^{-1} for MoS_2·NAPH and 190.2 m^2 g^{-1} for WS_2·NAPH. The observed differences in the surface area of MoS_2 and WS_2 exfoliated with sodium naphthalenide and butyllithium are in good agreement with the results obtained by microscopic techniques, where a substantially higher degree of exfoliation was observed for NAPH samples.

The magnetic measurements of butyllithium and sodium naphthalenide exfoliated TMDs were carried out using a SQUID magnetometer. At room temperature (T = 300 K) the field dependence of the magnetization was found to be given by a superposition of a diamagnetic moment proportional to the magnetic field (the corresponding susceptibilities X_D are listed in Table 2) and a small ferromagnetic (FM) contribution m_{FM}, for which the hysteresis loops are plotted in Fig. 6a.

The hysteresis curve is characterized by a very small coercivity of the order of 100 Oe and by the saturation magnetization m_S. The FM contribution is roughly independent of temperature. For samples WS_2·BuLi and MoS_2·BuLi the FM magnetization, if any, lies under a limit of 2.5×10^{-5} emu g^{-1} given by the accuracy of the measurement. At T = 2 K all samples exhibit a paramagnetic (PM) behaviour (Fig. 6b) which can be approximately described by the sum of the Brillouin contribution for spin S with the saturated value m_{PM0} and a small linear contribution with a susceptibility χ_1.

The value m_{PM0}, the estimated spin S as well as the susceptibility χ_1 are given in Table 2. In addition we performed a careful magnetic characterization of the starting bulk MoS_2 and WS_2. For both bulk materials the room temperature hysteresis curves corrected for a diamagnetic contribution with the susceptibility χ_D are shown in the ESI (Fig. SI8†). The ferromagnetic (FM) magnetization is observed only for the sample MoS_2, for which the value of the saturation magnetization m_S (see Table 2) reliably exceeds the error level 2.5×10^{-5} emu g^{-1}. In this case the hysteresis curve exhibits a finite remanent magnetization of 8.1×10^{-5} emu g^{-1} and a coercivity of 240 Oe. However this value is one order of magnitude lower compared to the exfoliated MoS_2. For the WS_2 sample we can also

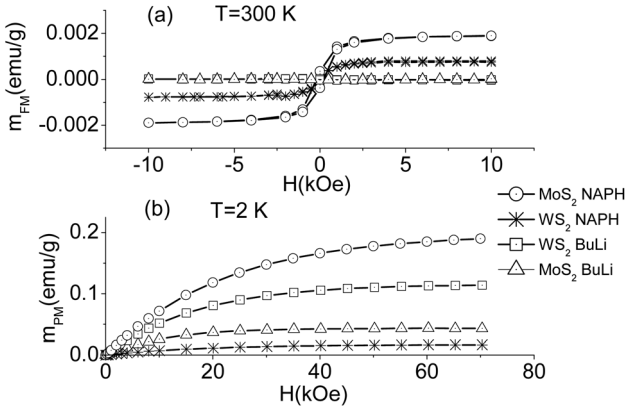

Fig. 6 (a) T = 300 K hysteresis loops for MoS_2 and WS_2, (b) T = 2 K, magnetization curves for MoS_2 and WS_2 (symbols – measured data, lines – calculation for S = 1 and the corresponding values m_{PM0}, χ_1 given in Table 2).

formally speak about the FM contribution but its value is lower than the error level. At the lowest temperature T = 2 K we measured the magnetization curves providing information about the paramagnetic (PM) contribution to the magnetic moment (Fig. 6b). The $m(H)$ curves can be well approximated by the sum of the PM Brillouin contribution for spin S = 2, g = 2 and a linear susceptibility χ_1 (Table 2). First we shall discuss the values of diamagnetic susceptibility contributions. The theoretical diamagnetic susceptibility for MoS_2 and WS_2 can be calculated using the data for Mo^{4+}, W^{4+} and S^{2-} ions.[38] This yields χ_D (MoS_2) = $-3.436.10^{-7}$ emu (g Oe)$^{-1}$ and χ_D (WS_2) = $-2.46.10^{-7}$ emu (g Oe)$^{-1}$. Whereas for the bulk materials MoS_2 and WS_2 we could speak about a rough agreement with the measured values of χ_D, a clear disagreement occurs for the sample MoS_2·NAPH (having the largest FM magnetization) where the measured value of χ_D is of the order of 10^{-8} emu (g Oe)$^{-1}$. The observed FM magnetization in the bulk is significantly lower compared to the material exfoliated with sodium naphthalenide. As far as the PM magnetization is concerned it is interesting that for the MoS_2 bulk sample the Brillouin approximation yields S = 2 in contrast to S = 1.5 for MoS_2·NAPH. This difference originates from the high degree of exfoliation and the 2H–1T phase transition observed by XPS. In the case of so small FM contributions, it is necessary to take into account the possible influence of impurities

mostly represented by iron. Starting from the data reported in the literature, we can infer that the FM saturation magnetizations m_S = 0.0019 emu g^{-1} and m_S = 0.0007 emu g^{-1} detected for MoS_2 and WS_2 correspond to the concentration of Fe impurities 8.6 and 3.18 ppm, respectively.[39]

For bulk MoS_2 and WS_2 no FM ordering has been observed so far to the best of our knowledge. However, detailed magnetic measurement of starting MoS_2 and WS_2 showed no or extremely weak magnetization (MoS_2) at room temperature and also the ferromagnetism of samples MoS_2·BuLi and WS_2·BuLi was below the detection limit of the SQUID device. This leads us to the conclusion that the room temperature ferromagnetism observed in sodium naphthalenide exfoliated MoS_2 and WS_2 is associated with several effects which take place during the TMD exfoliation. First we have to take into account the 2H–1T phase transition which is significantly larger compared to the samples exfoliated with butyllithium. The transformation of MoS_2 and WS_2 from 2H to 1T modification was observed by HR-TEM and well documented by XPS spectroscopy from deconvolution of Mo 3d and W 4f HR-XPS spectra, respectively. Moreover, a larger surface area imposes a higher concentration of edges, where a large amount of defects can be observed in HR-TEM images. Since NAPH samples possess a high degree of exfoliation, this will be one of the main factors necessary for the room temperature ferromagnetic ordering caused by the high concentration of edges related to a high degree of exfoliation and possibly also connected to the defects present on the edges. These defects may also lead to a PM contribution which superimposes on the intrinsic diamagnetic component. This manifests itself in the reduction of the measured susceptibility χ_D as was observed, *e.g.*, in the case of the sample MoS_2·NAPH. Let us mention that the FM state induced by defects was predicted for various types of defects in MoS_2 and also experimentally observed on nanostructured MoS_2 layers with a high concentration of defects.[35,40] We also have to note one possible origin of ferromagnetism, which has been recently reported on another transition metal dichalcogenide – $ReSe_2$. The room temperature ferromagnetism was observed on the wrinkled area of $ReSe_2$.[41] Such a wrinkling of the layers was also observed in the TEM images of MoS_2 and WS_2 sheets exfoliated with sodium naphthalenide. Although this feature was also observed in the MoS_2 exfoliated with butyllithium, a significantly lower degree of exfoliation led only to a minor influence on the magnetic behavior. Another interesting finding is the presence of a small PM contribution corresponding to the concentration of 10^{-3}–10^{-4} of PM centers with a spin S. The spin S = 1 could be connected with the occurrence of a spin-pairing of d^2 centers mentioned by other authors.[2] Our results suggest larger values of spins for the exfoliated WS_2 samples.

Conclusions

The detailed investigation of MoS_2 and WS_2 exfoliated using various alkali metal intercalating compounds like butyllithium and sodium naphthalenide yields materials with significant differences in the degree of exfoliation. The exfoliation using butyllithium predominantly resulted in a few layer materials, while the exfoliation using sodium naphthalenide led to almost complete exfoliation and formation of single layer TMDs. Such an intensive process of intercalation and subsequent exfoliation is associated with the 2H to 1T phase transition and formation of defects on the edges of TMD sheets. The presence of a metallic phase (1T) and formation of defects in the TMD structure can be responsible for the exotic ferromagnetic behavior which was observed up to room temperature. Even though the room temperature ferromagnetism is of the order of 1×10^{-3} emu g^{-1}, this effect was not observed in bulk MoS_2 and WS_2 or even in the butyllithium exfoliated material. Butyllithium exfoliated samples exhibit a significantly lower degree of exfoliation and subsequently a lower concentration of defects on the edges of individual sheets. This led us to draw a conclusion that the room temperature ferromagnetism is closely related to the structural disorder on the sheet edges and the presence of a conductive metallic phase. Our finding can have a strong impact on the future applications of transition metal dichalcogenides in the construction of novel spintronic devices.

Acknowledgements

J.L., O.J., D.S. and Z.S. acknowledge financial support from specific university research (MSMT no. 20/2015) and Czech Science Foundation (GACR no. 15-07912S). M.P. acknowledges Tier 2 grant (MOE2013-T2-1-056; ARC 35/13) from the Ministry of Education, Singapore. The result was developed within the CENTEM project, reg. no. CZ.1.05/2.1.00/03.0088, cofunded by the ERDF as part of the Ministry of Education, Youth and Sports OP RDI programme and, in the follow-up sustainability stage, supported through CENTEM PLUS (LO1402) by financial means from the Ministry of Education, Youth and Sports under the "National Sustainability Programme I".

Notes and references

1 L. Wang, Z. Sofer, J. Luxa and M. Pumera, *J. Mater. Chem. C*, 2014, **2**, 2887–2893.
2 R. Raja, P. Sudhagar, A. Devadoss, C. Terashima, L. K. Shrestha, K. Nakata, R. Jayavel, K. Ariga and A. Fujishima, *Chem. Commun.*, 2015, **51**, 522–525.
3 W. Kautek, F. Decker and H. Gerischer, *Phys. Status Solidi B*, 1984, **122**, 651–659.
4 R. H. Friend and A. D. Yoffe, *Adv. Phys.*, 1987, **36**, 1–94.
5 A. Splendiani, L. Sun, Y. Zhang, T. Li, J. Kim, C.-Y. Chim, G. Galli and F. Wang, *Nano Lett.*, 2010, **10**, 1271–1275.
6 C. Lee, H. Yan, L. E. Brus, T. F. Heinz, J. Hone and S. Ryu, *ACS Nano*, 2010, **4**, 2695–2700.
7 B. Schonfeld, J. J. Huang and S. C. Moss, *Acta Crystallogr., Sect. B: Struct. Sci.*, 1983, **39**, 404–407.

8 F. Wypych and R. Schollhorn, *J. Chem. Soc., Chem. Commun.*, 1992, 1386–1388.
9 R. Shidpour and M. Manteghian, *Nanoscale*, 2010, **2**, 1429–1435.
10 Y. Li, Z. Zhou, S. Zhang and Z. Chen, *J. Am. Chem. Soc.*, 2008, **130**, 16739–16744.
11 Y. Ma, Y. Dai, M. Guo, C. Niu, J. Lu and B. Huang, *Phys. Chem. Chem. Phys.*, 2011, **13**, 15546–15553.
12 J. Pütz and M. A. Aegerter, *J. Sol-Gel Sci. Technol.*, 2000, **19**, 821–824.
13 K.-K. Liu, W. Zhang, Y.-H. Lee, Y.-C. Lin, M.-T. Chang, C.-Y. Su, C.-S. Chang, H. Li, Y. Shi, H. Zhang, C.-S. Lai and L.-J. Li, *Nano Lett.*, 2012, **12**, 1538–1544.
14 J. Zhang, J. M. Soon, K. P. Loh, J. Yin, J. Ding, M. B. Sullivian and P. Wu, *Nano Lett.*, 2007, **7**, 2370–2376.
15 P. J. Grace, M. Venkatesan, J. Alaria, J. M. D. Coey, G. Kopnov and R. Naaman, *Adv. Mater.*, 2009, **21**, 71–74.
16 D. Gao, M. Si, J. Li, J. Zhang, Z. Zhang, Z. Yang and D. Xue, *Nanoscale Res. Lett.*, 2013, **8**, 129–129.
17 L. Cai, J. He, Q. Liu, T. Yao, L. Chen, W. Yan, F. Hu, Y. Jiang, Y. Zhao, T. Hu, Z. Sun and S. Wei, *J. Am. Chem. Soc.*, 2015, **137**, 2622–2627.
18 X. Mao, Y. Xu, Q. Xue, W. Wang and D. Gao, *Nanoscale Res. Lett.*, 2013, **8**, 430.
19 J. Kippling and R. B. Wilson, *J. Appl. Chem.*, 1960, **10**(3), 109–113.
20 A. Ambrosi, Z. Sofer and M. Pumera, *Small*, 2015, **11**, 605–612.
21 M. Chhowalla, H. S. Shin, G. Eda, L.-J. Li, K. P. Loh and H. Zhang, *Nat. Chem.*, 2013, **5**, 263–275.
22 J. Zheng, H. Zhang, S. Dong, Y. Liu, C. Tai Nai, H. Suk Shin, H. Young Jeong, B. Liu and K. Ping Loh, *Nat. Commun.*, 2014, 5.
23 D. Yang and R. F. Frindt, *J. Phys. Chem. Solids*, 1996, **57**, 1113–1116.
24 A. Berkdemir, H. R. Gutierrez, A. R. Botello-Mendez, N. Perea-Lopez, A. L. Elias, C.-I. Chia, B. Wang, V. H. Crespi, F. Lopez-Urias, J.-C. Charlier, H. Terrones and M. Terrones, *Sci. Rep.*, 2013, 3.
25 H. Terrones, E. D. Corro, S. Feng, J. M. Poumirol, D. Rhodes, D. Smirnov, N. R. Pradhan, Z. Lin, M. A. T. Nguyen, A. L. Elias, T. E. Mallouk, L. Balicas, M. A. Pimenta and M. Terrones, *Sci. Rep.*, 2014, 4.
26 P. Tonndorf, R. Schmidt, P. Böttger, X. Zhang, J. Börner, A. Liebig, M. Albrecht, C. Kloc, O. Gordan, D. R. T. Zahn, S. Michaelis de Vasconcellos and R. Bratschitsch, *Opt. Express*, 2013, **21**, 4908–4916.
27 D. Voiry, H. Yamaguchi, J. Li, R. Silva, D. C. Alves, T. Fujita, M. Chen, T. Asefa, V. B. Shenoy and G. Eda, *Nat. Mater.*, 2013, **12**, 850–855.
28 H. Li, Q. Zhang, C. C. R. Yap, B. K. Tay, T. H. T. Edwin, A. Olivier and D. Baillargeat, *Adv. Funct. Mater.*, 2012, **22**, 1385–1390.
29 A. Molina-Sánchez and L. Wirtz, *Phys. Rev. B: Condens. Matter*, 2011, **84**, 155413.
30 G. Eda, T. Fujita, H. Yamaguchi, D. Voiry, M. Chen and M. Chhowalla, *ACS Nano*, 2012, **6**, 7311–7317.
31 D. Yang, S. J. Sandoval, W. Divigalpitiya, J. Irwin and R. Frindt, *Phys. Rev. B: Condens. Matter*, 1991, **43**, 12053.
32 B. C. Windom, W. Sawyer and D. W. Hahn, *Tribol. Lett.*, 2011, **42**, 301–310.
33 X. Chia, A. Ambrosi, D. Sedmidubský, Z. Sofer and M. Pumera, *Chem. – Eur. J.*, 2014, **20**, 17426–17432.
34 W. Zhou, X. Zou, S. Najmaei, Z. Liu, Y. Shi, J. Kong, J. Lou, P. M. Ajayan, B. I. Yakobson and J.-C. Idrobo, *Nano Lett.*, 2013, **13**, 2615–2622.
35 J. Zhang, J. M. Soon, K. P. Loh, J. Yin, J. Ding, M. B. Sullivian and P. Wu, *Nano Lett.*, 2007, **7**, 2370–2376.
36 A. Y. S. Eng, A. Ambrosi, Z. Sofer, P. Šimek and M. Pumera, *ACS Nano*, 2014, **8**, 12185–12198.
37 K. Rida, S. Bouraoui and S. Hadnine, *Appl. Clay Sci.*, 2013, **83–84**, 99–105.
38 Landolt-Börnstein: *Group II, Moleculs and Radicals*, ed. W. Martienssen, 1986, vol. 16, p. 402.
39 P. Esquinazi, A. Setzer, R. Höhne, C. Semmelhack, Y. Kopelevich, D. Spemann, T. Butz, B. Kohlstrunk and M. Lösche, *Phys. Rev. B: Condens. Matter*, 2002, **66**, 024429.
40 R. Shidpour and M. Manteghian, *Nanoscale*, 2010, **2**, 1429–1435.
41 S. Yang, C. Wang, H. Sahin, H. Chen, Y. Li, S.-S. Li, A. Suslu, F. M. Peeters, Q. Liu, J. Li and S. Tongay, *Nano Lett.*, 2015, **15**, 1660–1666.